

SAMPLING STRATEGIES IN MULTIPLE-IMAGE RADIOGRAPHY

Keivan Majidi¹, Jovan G. Brankov¹, and Miles N. Wernick^{1, 2}

¹ECE Dept., Illinois Institute of Technology, Chicago, IL 60616, USA

²Dept. of Biomedical Engineering, Illinois Institute of Technology, Chicago, IL 60616, USA

ABSTRACT

Multiple-Image Radiography (MIR) is an analyzer-based phase-sensitive x-ray imaging method, which is a potential alternative to conventional radiography. MIR simultaneously generates three planar images containing information about scattering, refraction and absorption properties of the object. These parametric images are acquired by sampling the angular intensity profile of the beam passing through the object at different positions of the analyzer crystal. Like many of the modern imaging techniques, MIR is a computing imaging method and the noise in MIR, in addition to the imaging conditions, depends also on the estimation of the parameters. In this work, we use Cramér-Rao lower bound to quantify the noise in MIR estimated images and investigate the effect of different sampling strategies at the analyzer on this bound. We also evaluate the performance of an estimator with respect to this bound.

Index Terms— Multiple-Image Radiography, Cramér-Rao Lower Bound, Diffraction-Enhanced Imaging, Phase Sensitive Imaging

1. INTRODUCTION

Multiple image radiography (MIR) [1] is a planar imaging method which is an improvement of the DEI [2] technique. MIR can simultaneously calculate three different parametric images from a set of measurements acquired using the system shown in Figure 1. This imaging system, also known as a Bonse-Hart camera [3], includes a monochromatic x-ray beam and an analyzer crystal. The parametric images generated in MIR are attenuation, refraction and ultra-small-angle x-ray scatter (USAXS). The attenuation image shows a combination of absorption and Compton-scatter extinction. The refraction image in MIR shows the integrated effect of refractive index variations along the beam path and is suitable for visualizing soft tissues with small absorption coefficients, e.g. tendons and cartilages. The USAXS image represents the sub-pixel textural structure of the object and is suitable for observing textural soft tissues such as breast tumors or calcaneal fat pad. It should be noted that similar methods have also been proposed independently in [4] and [5].

Because the contrast of the refraction and scatter images does not rely on absorption of x-rays by the object, MIR can be performed at higher energies than conventional mammography (e.g., using a tungsten anode rather than molybdenum); at these higher energies, radiation exposure to the patient is low and refraction contrast remains high for soft tissue imaging.

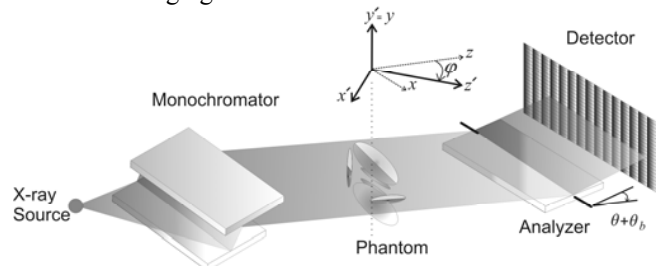


Figure 1. MIR Imaging System

Because MIR is a fairly new technique, its basic properties are as yet unknown. For example, the noise performance has not been fully described, and it is not known how best to acquire the data (specifically, how analyzer positions must be used). This paper seeks to answer both questions.

In our previous work [6], the noise in estimated MIR images was quantified by using the Cramér-Rao lower bound (CRLB) [7] for each image. CRLB is the minimum bound on the variance of any unbiased estimator and defines the best noise performance that can be obtained in parameter estimation from a source of data. In that work, we made a simplifying assumption that the MIR images are computed independently of one another, which is never the case in practice; therefore, our earlier results were somewhat unrealistic. In this work, we improve the noise quantification by using the CRLB for vector estimators and used this bound to investigate the noise performance in MIR data acquisition procedure. We then evaluate the performance of a simple estimator which was introduced in [8] and compared its variance to the bound in order to seek a minimum-variance unbiased (MVU) estimator.

2. IMAGING MODEL

In MIR imaging system shown in Figure 1, the object is first illuminated with a collimated, monochromated X-ray

beam obtained using a pair of silicon (Si 333) crystals. While the X-ray beam passes through the object, it will be affected by the object properties, which will change the beam angular intensity profile (AIP), i.e. x-ray power as a function of the angular direction of propagation. Next, an analyzer crystal, which is a narrow angular filter, is used to analyze the beam AIP. This angular filter passes only beam components that are traveling at or near its Bragg angle, θ_b . Since the angular range for this filter is in the order of microradians we can assume that there is no cross talk between the adjacent pixels on the detector and the imaging could be considered as pixel-by-pixel. By measuring the intensity at different angular positions of the analyzer, θ , the AIP of the beam can be effectively measured. The AIP for each pixel can be used to extract the information about attenuation, refraction and USAXS which will be described later.

First, we characterize the imaging system by $R(\theta)$ which is the AIP that would be measured in absence of the object on the detector plane. Then we can write the beam AIP with the presence of the object on the detector surface as:

$$g(\theta) = R(\theta) * f(\theta) \quad (1)$$

where $*$ denotes convolution with respect to θ and $f(\theta)$ represents the *object function* which is the impulse response of the object, i.e. the AIP that would be measured if the object were illuminated with a perfectly collimated beam having an AIP that is a Dirac delta function. For the object function, we use the model proposed in [9] which can be written as:

$$f(\theta) = v_1 \frac{1}{\sqrt{2\pi v_3}} \exp\left(-\frac{(\theta - v_2)^2}{2v_3}\right) \quad (2)$$

where $v_1 = \int_l A(\bar{r}) d\bar{l}$ is the attenuation caused by the object and is the line integral of absorption coefficient, $A(\bar{r})$, along the beam path l , $v_2 = -\int_l \frac{\partial}{\partial y'} n(\bar{r}) d\bar{l}$ is the angular shift of the beam centroid which is the integral of refractive index gradient, $\frac{\partial}{\partial y'} n(\bar{r})$, $v_3 = \int_l usaxs(\bar{r}) d\bar{l}$ is the angular beam divergence and is the integral of the USAXS parameter, $usaxs(\bar{r})$ and $\bar{r} = (x', y', z')^T$.

Now the expected value of the measured discrete AIP on the detector can be modeled as:

$$\bar{g}_m = E[g[m]] = \frac{I_0}{M} g(\theta_m) \quad (3)$$

where $m = 1, 2, \dots, M$ represents the index of the analyzer angle, θ_m , I_0 is the maximum count of photons per pixel for $M=1$ and $E[.]$ denotes the expected value. Since we envision practical implementation of MIR using the conventional x-ray tubes, where flux may be the performance constraint, we assume that the data is photon-

limited so Poisson noise will be the dominant noise source in MIR images [1]. Under this noise model the likelihood function of the data is given by:

$$p(\mathbf{g}; \mathbf{v}) = \prod_{m=1}^M \frac{\bar{g}_m^{g[m]} e^{-\bar{g}_m}}{g[m]!} \quad (4)$$

where $\mathbf{g} = (g[1], g[2], \dots, g[M])$ is the data vector and $\mathbf{v} = (v_1, v_2, v_3)$ is the MIR parameter vector to be estimated.

3. SAMPLING STRATEGIES

3.1. CRLB Theorem for MIR Parameters

To investigate the effect of noise on each estimated parameter we consider the theoretical lower bound (CRLB) on the noise variance for unbiased estimators. The CRLB theorem [7] for vector estimation states that the variance of any unbiased estimator, \hat{v}_i of an element, v_i of parameter vector \mathbf{v} is bounded by:

$$\text{Var}(\hat{v}_i) \geq \{\mathbf{I}^{-1}(\mathbf{v})\}_{ii} \quad (5)$$

in which $\mathbf{I}(\mathbf{v})$ is the Fisher information matrix which its elements are defined as:

$$\{\mathbf{I}(\mathbf{v})\}_{i,j} = -E\left[\frac{\partial^2}{\partial v_i \partial v_j} \ln p(\mathbf{g}; \mathbf{v})\right] \quad (6)$$

By using (1)-(4) in (6) we can derive the following Fisher information matrix for MIR parameters:

$$\mathbf{I}(\mathbf{v}) = \begin{bmatrix} \sum_{m=1}^M \frac{g_m}{v_1^2} & \sum_{m=1}^M \frac{h_m - v_2 g_m}{v_1 v_3} & \sum_{m=1}^M \frac{q_m - v_3 g_m}{2v_3^2 v_1} \\ \sum_{m=1}^M \frac{h_m - v_2 g_m}{v_1 v_3} & \sum_{m=1}^M \frac{(h_m - v_2 g_m)^2}{v_3^2 g_m} & \sum_{m=1}^M \frac{(h_m - v_2 g_m)(q_m - v_3 g_m)}{2v_3^2 g_m} \\ \sum_{m=1}^M \frac{q_m - v_3 g_m}{2v_3^2 v_1} & \sum_{m=1}^M \frac{(h_m - v_2 g_m)(q_m - v_3 g_m)}{2v_3^2 g_m} & \sum_{m=1}^M \frac{(q_m - v_3 g_m)^2}{4v_3^4 g_m} \end{bmatrix}$$

where:

$$h_m \triangleq \left[\frac{I_0}{M} R(\theta) * \theta f(\theta; \mathbf{v}) \right]_{\theta=\theta_m}$$

$$q_m \triangleq \left[\frac{I_0}{M} R(\theta) * (\theta - v_2)^2 f(\theta; \mathbf{v}) \right]_{\theta=\theta_m}$$

In our problem the bound cannot be computed analytically in this form, however, we can compute the bounds numerically for any given parameter vector.

3.2. Effect of Sampling on CRLB

In imaging a particular object where the rocking curve is known, the most important factor affecting the noise is the angular sampling pattern of the analyzer crystal. In this section we analyze the behavior of CRLB as we increase the

number of angular samples, M , in the analyzer. We consider the sampling pattern at the analyzer, $\theta_M = (\theta_1, \theta_2, \dots, \theta_M)$, to be symmetrical around $\theta = 0$ and distributed in the range of $[-6:6]$ μrad . We estimate the CRLB for each sampling pattern as:

$$\text{CRLB}_i(\theta_M) = E\left[\left\{\mathbf{I}^{-1}(\mathbf{v}; \theta_M)\right\}_{ii}\right] \quad (7)$$

where $E[\cdot]$ represents the expectation over the probability density function (pdf) of MIR parameter vector, \mathbf{v} . Taking the expectation in (7) is an intractable problem. Therefore, we approximate the expectation by the arithmetic average of the CRLB over the MIR parameters in a simulation phantom which is shown in Figure 2. The parameter values in the phantom are assigned to match the corresponding values form a human thumb joint study.

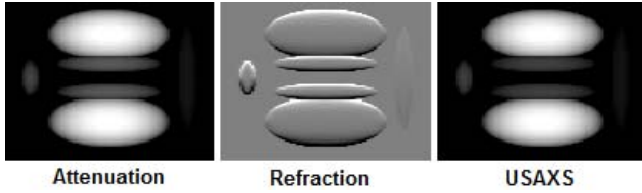


Figure 2. MIR phantom based on a human thumb

We estimate the expectation in (7) by:

$$\text{CRLB}_i(\theta_M) = \frac{1}{C} \sum_{c=1}^C \left\{ \mathbf{I}^{-1}(\mathbf{v}^c; \theta_M) \right\}_{ii} \quad (8)$$

where $\mathbf{v}^c, c=1, \dots, C$ represents the values of the MIR parameter vector, \mathbf{v} , at the c^{th} pixel in the phantom. The changes in CRLB for different number of samples are shown in Figure 3.

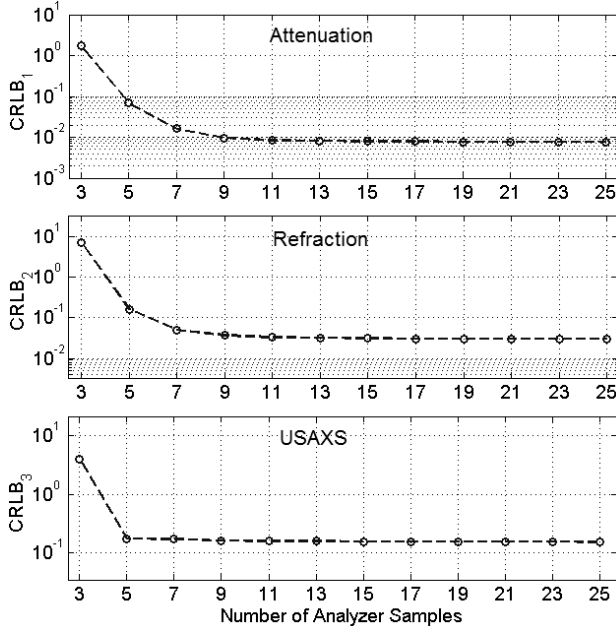


Figure 3. CRLB vs. number of samples for MIR parameters

We assumed $I_0 = 750$ photons/pixel which corresponds to the maximum count of 100 photons/pixel for $M=25$. We can see the improvement in CRLB as we increase the number of analyzer samples. However, after 11 samples the improvement in the bound becomes small and there is almost no benefit in acquiring more than 11 samples from the analyzer for an MVU estimator.

4. VARIANCE OF ESTIMATION

The graphs in Figure 3 can also be used to evaluate the performance of each estimator in MIR. Here, we chose an estimator for MIR parameters [8] in order to investigate the effect of the sampling pattern on the estimation variance. First, we describe the estimation procedure:

We define the normalized AIP as:

$$G[m] = g[m] / \sum_{m=1}^M g[m] \quad (9)$$

and the total intensity that would be measured in the absence of the object will be denoted as:

$$I'_0 = \frac{I_0}{M} \sum_{m=1}^M R[m] \quad (10)$$

where $E[R[m]] = R(\theta_m)$, measured on any pixel in the detector plane in the absence of object. We also define the AIP shift of the imaging system by:

$$\Delta R_\theta = \frac{1}{I'_0} \sum_{m=1}^M (m - \frac{M+1}{2}) R[m] \Delta \quad (11)$$

where $\Delta = \frac{12}{M-1} \mu\text{rad}$ is the angular spacing between the measurements. Now we can estimate the three MIR parameters at each pixel on the detector as follows:

$$v_1 = -\ln \frac{\sum_{m=1}^M g[m]}{I'_0} \quad (12)$$

$$v_2 = \sum_{m=1}^M (m - \frac{M+1}{2}) G[m] \Delta - \Delta R_\theta \quad (13)$$

$$v_3 = \sum_{m=1}^M \left[(m - \frac{M+1}{2}) \Delta - v_2 \right]^2 G[m] - \frac{1}{I'_0} \sum_{m=1}^M \left[(m - \frac{M+1}{2}) \Delta - \Delta R_\theta \right]^2 R[m] \quad (14)$$

We calculated the variance of estimation by using 1000 noise realization for each pixel in the phantom and averaging the calculated variances over all pixels in the image. Using the same noise realization, we also calculated the Mean Square Error (MSE) and the squared bias of the estimation. The results are shown in Figure 4. We can see in these graphs that this estimator is highly biased for low number of samples, hence, making the variance lower than the unbiased CRLB. But after 11 samples the bias of the estimation becomes negligible compare to the variance.

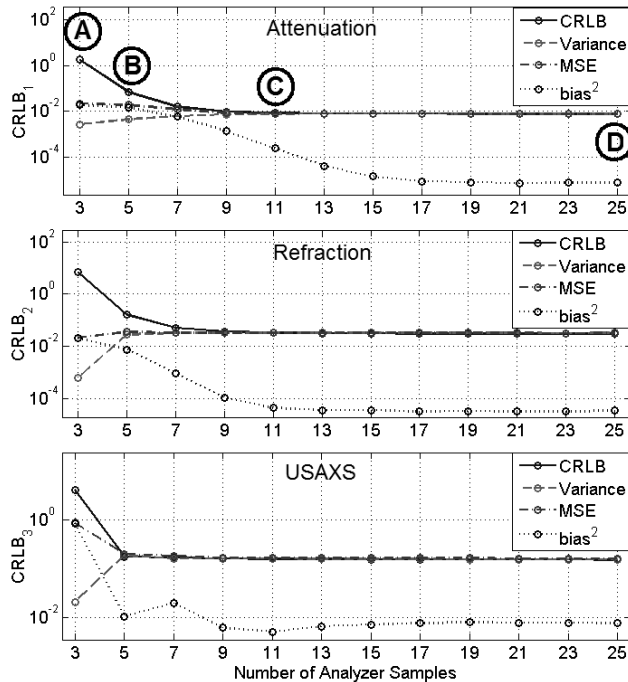


Figure 4. Variance, MSE and squared-bias of the estimator vs. different number of samples compared to CRLB.

Another interesting result in Figure 4 is that not only this estimator is fairly unbiased after 11 samples; it also achieves CRLB and hence is an MVU estimator. The results confirm our previous conclusion that there is no decrease in the variance of estimation after 11 samples.

In order to see the above results in a visual form, the estimated images for 4 different numbers of samples are shown in Figure 5. The image rows are marked by letters A, B, C and D which correspond to the same letters on the attenuation graph in Figure 4.

5. CONCLUSION

To investigate the effect of sampling strategies on the noise in MIR images we have derived the vector form of the Cramér-Rao lower bound for MIR parameters. By assuming uniform sampling and using probability density function of MIR parameters in a phantom study, we numerically estimated this bound for different numbers of samples. We found that by using more than 11 samples from the analyzer there is not much improvement in CRLB values and we can save the imaging time by not measuring more than 11 samples from the analyzer.

We also evaluated the performance of a simple and fast estimator and compared the results to the CRLB values. Presented results showed that for uniform sampling, this estimator asymptotically achieves the CRLB after 11 samples and becomes a minimum-variance unbiased estimator.

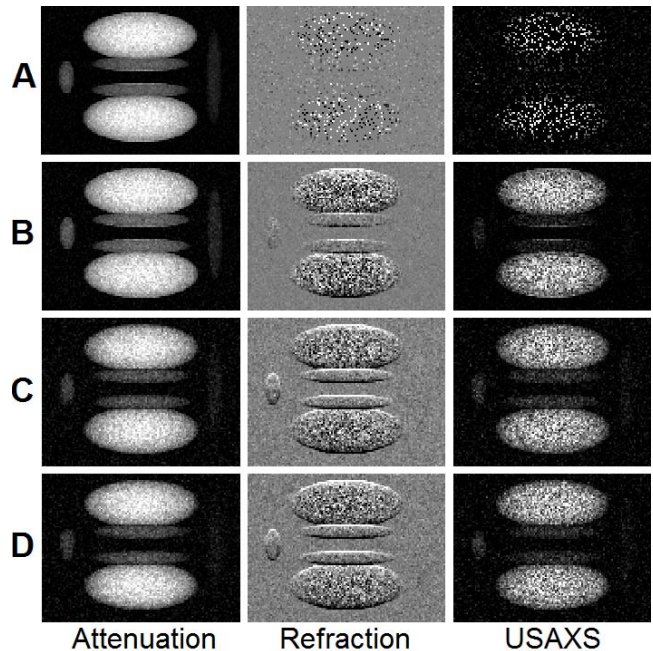


Figure 5. Estimated MIR images using different number of samples in analyzer.

In future work, we seek to minimize the CRLB value by deforming the sampling pattern from uniform and find an unbiased estimator in the case of non-uniform sampling that can achieve the CRLB. We will also investigate the effect of sampling strategies on three dimensional MIR images reconstructed by CT-MIR [8].

ACKNOWLEDGMENTS

This research was supported by NIH/NIAMS Grant No. AR48292 and NIH/NCI Grant No. CA111976.

6. REFERENCES

- [1] M. N. Wernick *et al*, "Multiple-Image Radiography," *Phys. Med. Biol.*, vol. 48, pp. 3875-3895, 2003.
- [2] D. Chapman *et al*, "Diffraction Enhanced X-ray Imaging," *Phys. Med. Biol.*, vol. 42, pp. 2015-2025, 1997.
- [3] U. Bonse, M. Hart, *Appl. Phys. Lett.*, vol. 7, 1965, p. 238.
- [4] E. Pagot *et al*, "A Method to Extract Quantitative Information in Analyzer-Based X-ray Phase Contrast Imaging" *Appl. Phys. Lett.*, vol. 82, pp. 3421-3, 2003
- [5] L. Rigon *et al*, "A New DEI Algorithm Capable of Investigating Sub-Pixel Structures" *J. Phys. D: Appl. Phys.*, vol. 36, pp. 107-112, 2003
- [6] B. Marquet *et al*, "Noise and Sampling Analysis for Multiple Image Radiography" *IEEE Int. Symp Bio Imag.*, 2006, pp. 1232-1235.
- [7] Kay, S. M. *Fundamental of Statistical Signal Processing: Estimation Theory*. New-York: Prentice-Hall (1993)
- [8] J. G. Brankov *et al*, "A computed tomography implementation of multiple-image radiography," *Med. Phys.*, vol. 33, pp. 278-289, 2006.
- [9] G. Khelashvili *et al*, "A physical model of multiple image radiography," *Phys. Med. Biol.*, vol. 51, pp. 221-236, 2006.